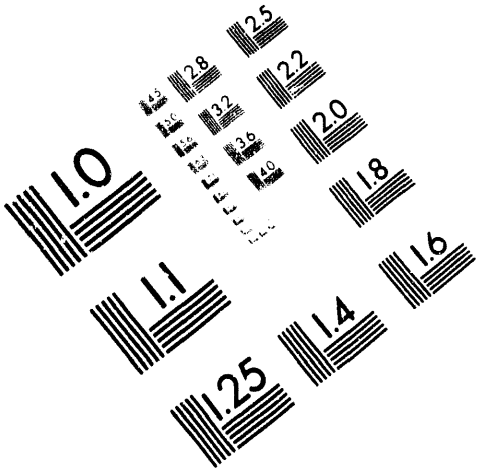

**Association for Information and Image Management**

1100 Wayne Avenue, Suite 1100
Silver Spring, Maryland 20910

301/587-8202

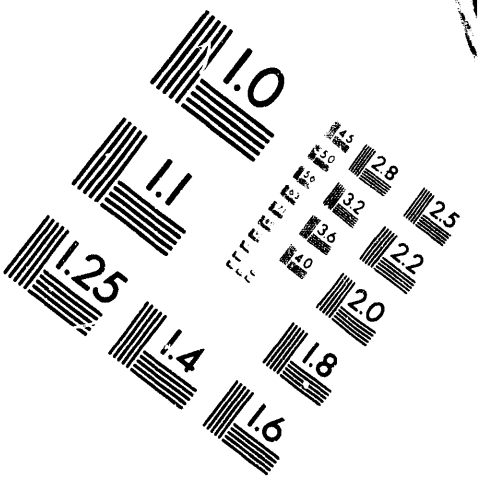

Centimeter

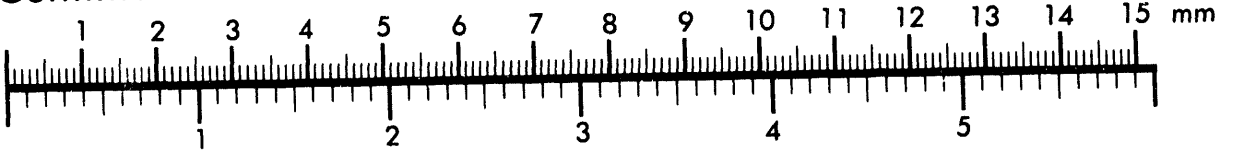

Inches

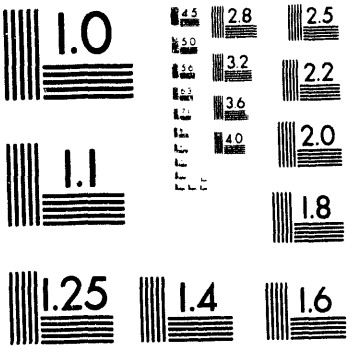

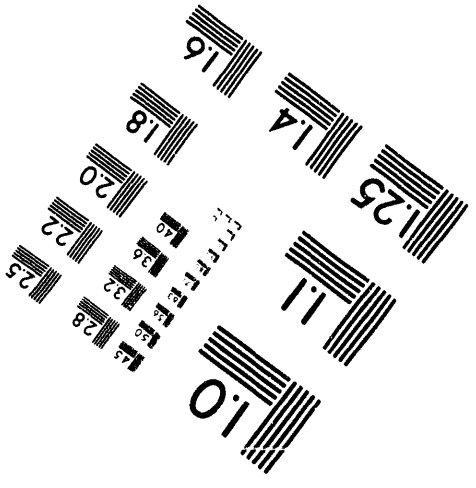

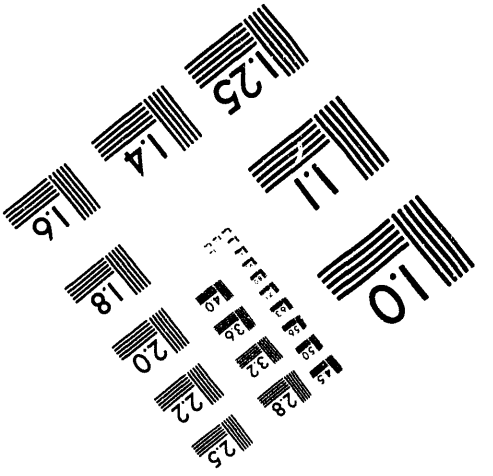

MANUFACTURED TO AIIM STANDARDS
BY APPLIED IMAGE, INC.

1 of 1

12
7-16-93 JSD

UCRL-ID-112219

# Evaluation of Materials Proposed for the Construction of the Plasma Electrode Pockels Cell (PEPC) on Beamlet

Dave Roberts, Calvin Robb,
James De Yoreo, Jeff Atherton

November 1992

Lawrence Livermore National Laboratory

This is an informal report intended primarily for internal or limited external distribution. The opinions and conclusions stated are those of the author and may or may not be those of the Laboratory.
Work performed under the auspices of the U.S. Department of Energy by the Lawrence Livermore National Laboratory under Contract W-7405-Eng-48.

DISCLAIMER

This document was prepared as an account of work sponsored by an agency of the United States Government. Neither the United States Government nor the University of California nor any of their employees, makes any warranty, express or implied, or assumes any legal liability or responsibility for the accuracy, completeness, or usefulness of any information, apparatus, product, or process disclosed, or represents that its use would not infringe privately owned rights. Reference herein to any specific commercial products, process, or service by trade name, trademark, manufacturer, or otherwise, does not necessarily constitute or imply its endorsement, recommendation, or favoring by the United States Government or the University of California. The views and opinions of authors expressed herein do not necessarily state or reflect those of the United States Government or the University of California, and shall not be used for advertising or product endorsement purposes.

This report has been reproduced
directly from the best available copy.

Available to DOE and DOE contractors from the
Office of Scientific and Technical Information
P.O. Box 62, Oak Ridge, TN 37831
Prices available from (615) 576-8401, FTS 626-8401

Available to the public from the
National Technical Information Service
U.S. Department of Commerce
5285 Port Royal Rd.,
Springfield, VA 22161

# EVALUATION OF MATERIALS PROPOSED FOR THE CONSTRUCTION OF THE PLASMA ELECTRODE POCKELS CELL (PEPC) ON BEAMLET

DAVE ROBERTS, CALVIN ROBB,
JAMES DE YOREO, JEFF ATHERTON

MASTER

# OUTLINE


**1.0** Introduction

**2.0** Survey of Materials: Outgassing performance and electrical properties of cell materials

**3.0** Optical Switch Assembly

- **3.1** Technique to evaluate crystal encapsulation
- **3.2** Analysis of encapsulation

**4.0** Electrode Sputtering Issues

- **4.1** Evaluating sputtering rates of cathode materials
- **4.2** Experiment matrix
- **4.3** Calibration of deposited film
- **4.4** Laser damage evaluation
- **4.5** Confirmation of reactive gas process
- **4.6** Introduction to carbon graphite cathode materials

**5.0** Materials Evaluation Experiment Apparatus

- **5.1** Evaluation of the silicone encapsulant
  - **5.1.1.** Analysis
  - **5.1.2** Effects of ultraviolet radiation
  - **5.1.3.** Change in physical properties
  - **5.1.4** Affects of ozone ($O_3$) and arcing
- **5.3** Evaluation of Macor and Mykroy Switch materials
- **5.4** Evaluation of Polyethylene Switch materials
  - **5.4.2.** Effect of discharge arcing

**6.0** Conclusion

- **6.1** Acknowledgments

**7.0** References

## 1.0 Introduction

The proposed upgrade of the NOVA laser system at Lawrence Livermore National Laboratory (LLNL) employs a multipass architecture that requires an optical switch to emit the laser light at the appropriate fluence. This Pockels cell-based optical switch does not use traditional ring or thin-film electrodes because of the large aperture and high fluence of the laser system. Rather, it uses a plasma electrode Pockels cell with a KD*P crystal as the electro-optical medium. A discharge plasma is formed on each side of the electro-optic crystal and high voltage is applied across the crystal through the plasma electrode to initiate optical switching. The development of this electro-optical switch was demonstrated by Goldhar and Henesian.[1]

In October 1991 we began evaluating materials suggested for the construction of the large aperture plasma electrode optical switch. Previous experiments done by Goldhar and Henesian in developing the switch suggested that switching performance could be significantly affected by the deterioration of cell materials. In addition we were concerned that the decomposition of these materials and volatiles produced by the plasma would deposit on the optical surface, lowering transmission and the damage threshold of the KD*P.

The final prototype switch tested used polyethylene for the switch body, Mykroy for the mid-plane and a silicone vulcanite to encapsulate the KD*P crystal. The encapsulant easily compensated for the effect of assembling the optical switch and we measured no strain-induced birefringence in the crystal after encapsulation. Oxygen was eventually added to the plasma to react with the sputtered carbon from the cathode and produce a gaseous effluent. As an added benefit, the production of ozone absorbed most of the ultra violet radiation affecting the encapsulant. All the materials tested decomposed and produced volatiles, although we have seen no change in the damage threshold of exposed optical surfaces tested to date.

The following is an evaluation of the recommended materials for major cell components using published manufacturers data, experimental results from our Material Evaluation Apparatus, and outgassing performance and sputtering data produced at the Laboratory's Vacuum Process Lab (VPL).

## 2.0 Survey of Cell Materials: Outgassing Performance and Electrical Properties of Cell Materials

Characterizing the evolution of gas from cell materials was necessary to properly design the switch vacuum system and critical in evaluating plasma performance. Tests done in the Vacuum Process Lab were conducted in a baked-out ultra high vacuum vessel using the throughput method for determination of evolved gas load.[2] In each test, the specimen was placed in a vessel which is connected to the vacuum pump stack by a tube with a 0.46 mm diameter orifice. During the test, the system was evacuated, and we monitored pressure readings on both sides of the orifice. Using a calculated value of the orifice conductance (C) and the measured pressures ($P_1$ and $P_2$) we calculated the outgassing rate using the equation:

$$Q = C\ (P_1 - P_2)$$

Where Q is the outgassing rate, expressed in Torr-liters/sec, the value of C is 0.019, and $P_1$ is the pressure measured on the sample side of the orifice. The outgassing rate measured was divided by the specimen geometrical surface area to yield outgassing rate per square centimeter of surface area. We also recorded the process temperature when applicable and volatile gas species for each material.

| Material | Torr•liters/second•cm$^2$ | Process temperature, °c | Volatile gasses |
|---|---|---|---|
| Macor | $3.0 \times 10^{-11}$ | 200 | $H_2O$, CO |
| Anodize Aluminum | $2.5 \times 10^{-10}$ | 150 | $H_2O$, CO, $CO_2$ |
| KDP ($SiO_2$ coated) | $3.0 \times 10^{-9}$ | N/A | not recorded |
| Mykroy | $9.0 \times 10^{-9}$ | 200 | $H_2O$ |
| UHMW polyethelene | $1.5 \times 10^{-8}$ | 100 | $H_2O$, CO |
| Acrylic (Lucite) | $4.5 \times 10^{-7}$ | 40 | $H_2O$, CO, $Co_2$ |
| Dow Corning 93-500 silicone | $1.0 \times 10^{-6}$ | N/A | $H_2O$, CO, $CO_2$ |
| Conap TU-500 urethane | $1.0 \times 10^{-5}$ | N/A | $H_2O$ |

**Table 1.** Outgassing rate, process temperature and volatiles of the materials suggested for the construction of the large aperture optical switch.

Because of the proposed switch geometry and the large cross sectional area needed to support the KD*P crystal, we surveyed the published dielectric strength of the potential cell materials given in Table 2. Only the anodized aluminum would not meet the nominal 8.5 kV @ 120 ns switch pulse.

| Material | Manufacturer | Dielectric V/.001" |
|---|---|---|
| Macor | Dow Corning | 3000 |
| 93-500 Silicone | Dow Corning | 570 |
| UHMW Ployethelene | Polymer Corp. | 500 |
| Conap TU-500 Urethane | Dupont | 480 |
| Mykroy | Mycalex Corp. | 375 |
| Anodize Aluminium | Sanford Process Corp. | 625* |

* 6000 volts maximum

**Table 2.** Dielectric strengths of the material suggested for the construction of the large aperture optical switch.

## 3.0 Optical Switch Assembly

Assembly of the optical switch could be critical if precise tolerances were not maintained. Previous designs sandwiched the encapsulated crystal in a middle plane between two low pressure plasma chambers.[1] With this design and other designs we considered, there was the possibility that non-uniform loads could induce strain in the KD*P crystal if the material selected for encapsulation was not compliant.

### 3.1 Technique to Evaluate Crystal Encapsulation

To test the affects of encapsulation we used a circular polarimeter similar to that described by Hayakawa,[3] designed to measure depolarization in the crystal due to strain induced birefringence. We mapped the depolarization produced by of the KD*P crystal prior to encapsulation to establish a baseline for the strain birefringence level. We then encapsulated the crystal using a precision mold technique.[4]

## 3.2 Analysis of Encapsulation

Figure 1 shows an average percent depolarization loss of 0.0043% for transmitted 1.06 μm light and a maximum depolarization loss of 0.058% for the free-standing crystal. After the encapsulation, the losses were 0.0021% and 0.086% respectively, which suggest that encapsulating the crystal actually more uniformly supports the KD*P than the free-standing technique.

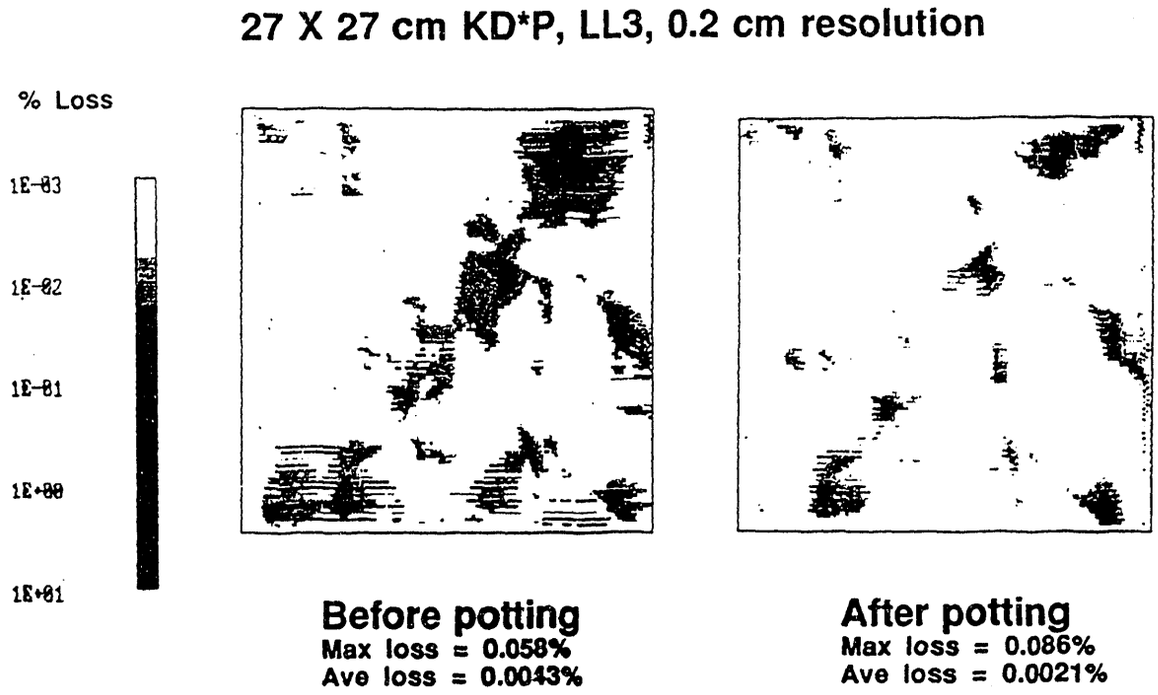


**Figure 1.** After encapsulation the average depolarization loss is reduced while the maximum loss has a slight increase. Recorded values are within the limits of calibration.

Once we were confident that the encapsulant did not induce strain in the crystal, we then used the assembled mid-plane to test the compliance of the encapsulant. By deflecting the mid-plane at the center of the bottom edge, normal to the incident surface by 0.050 inch, we measured the strain induced birefringence caused by the deflection. Figure 2 shows the affect of deflection to be within the calibration limits of our system. With an average loss in transmission still only at 0.0078% and a maximum loss of 0.067% this encapsulant easily compensates for the affect of assembling the optical switch.

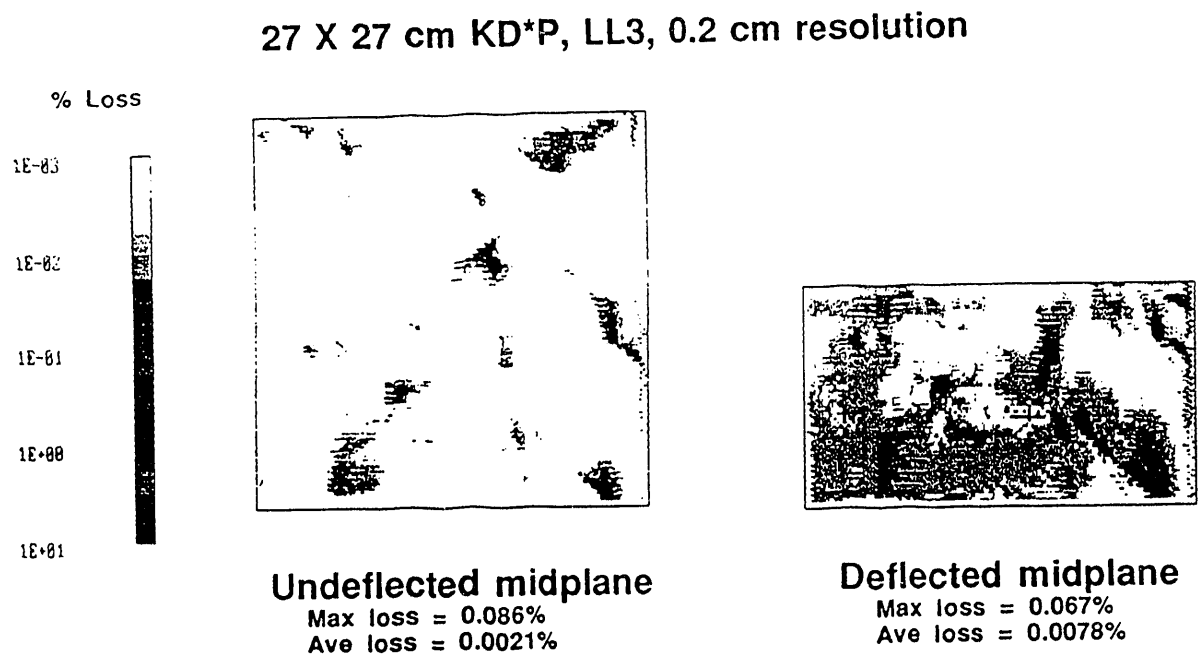


**Figure 2.** The average depolarization increases slightly when deflecting the mid plane by 0.050 in. The silicone encapsulant easily compensates for the affect of assembling the optical switch. Only the lower half of the crystal was mapped for the deflected midplane.

## 4.0 Electrode Sputtering Issues

The first prototype Pockels cell[1] was fabricated from cast acrylic with sheet stainless steel electrodes. After several hours of operation we could see a clear indication that the cell material was being eroded by ions, electron or UV radiation. Initially we felt that sputtering of cell material would be an important area to investigate; however, in recently designed cells this became a critical performance issue when planar magnetrons were used to improve the switching performance of the cathode electrode. When cathode materials such as stainless steel and molybdenum were used with these magnetically enhanced electrodes we eventually deposited enough sputtered material onto the crystal, lowering its damage threshold and affecting switch performance.

### 4.1 Evaluation of Sputtering Rates of Cathode Materials

To better understand the sputtering relationship of the cathode material and the magnetically enhanced electrode, we conducted a matrix of experiments to determine the sputtering yields of various cathode materials at the Vacuum Process Lab (VPL). Figure 3 shows published data of the relative sputtering yield for various elements in argon, at the voltage of interest. Materials like molybdenum and tungsten which have historically been used for electrodes exhibit low sputtering yields, however, carbon clearly stands out for its low sputtering yield and offered the possibility of

chemically reacting with the plasma gases to produce a gas that could be pumped away. If the addition of a small amount of oxygen or hydrogen were added to the helium plasma and did not affect the switching performance, this reactive gas process would likely yield carbon monoxide (CO) and carbon dioxide ($CO_2$) with oxygen, and methane ($CH_4$) with hydrogen and prevent deposition of sputtered material onto the crystal.

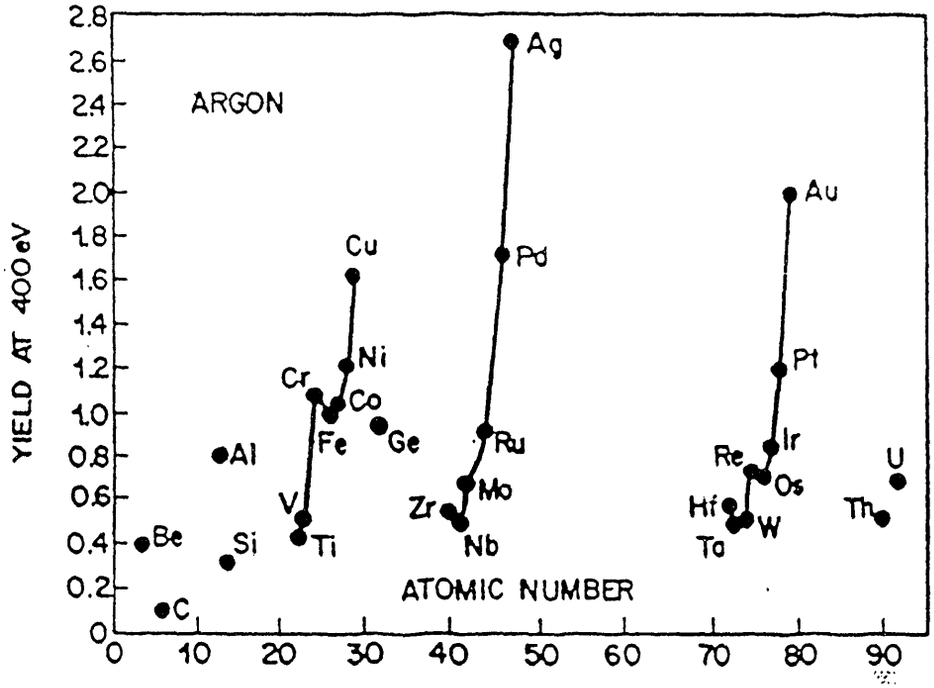


**Figure 3.** Sputtering yield as a function of substrate atomic number using 400V argon ion bombardment. Carbon clearly stands out for its low sputtering yield. (N. Laegried and G.K. Wehner, J. Appl. Phys. 32; 365 (1961).

Sputtering yield is heavily dependent on the ion source, experimental geometry and plasma parameters. To most effectively evaluate these materials, our experimental setup attempted to simulate the operating conditions of the Pockels cell. To evaluate the sputtering rate of the different cathode materials, we used a 2 inch diameter commercially produced magnetron sputtering source and a dynamically pumped high vacuum system. Because sputter film deposition is inversely proportional to distance, we used two substrates to ensure that we would have comparable data for materials with a large difference in sputtered deposition. Figure 4 shows the position of the two sample glass substrates with half the surface masked. The vertical substrate was nominally located 2.5 inches from the magnetron and off to one side of the diameter of the cathode target material. The horizontal substrate was twice the distance from the magnetron and directly over the target material. By sputtering each cathode material for the same period of time, we were then able to compare the sputtered deposition of these materials by measuring the height of the step created when the substrate masks were removed.

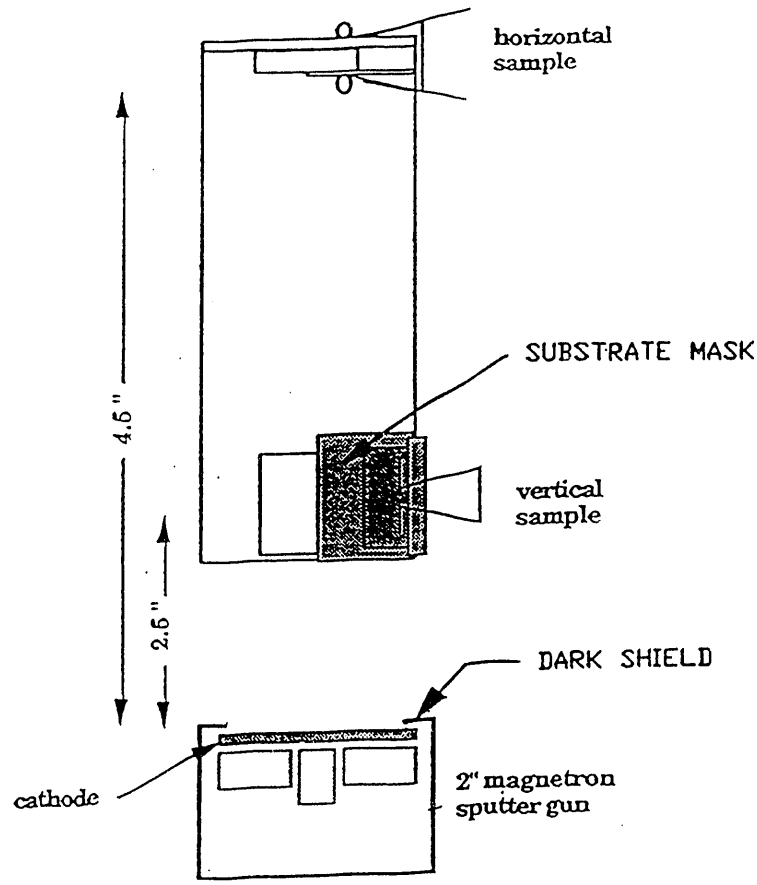


**Figure 4.** Experimental setup at Vacuum Process Laboratory uses a magnetron sputtering source with witness plates. Cathode material deposited on the witness plate sample is measured to determine deposition rate.

During the sputtering test we maintained the plasma pressure @ 5 X $10^{-2}$ torr by dynamically pumping the vacuum chamber with a turbomolecular vacuum system, while continuing to flow the working gas. We regulated the discharged current at 200 ma and recorded the operating voltages for each cathode material. To ensure a measurable difference in the sputtering yield we sputtered for nominally 4 hours with each material.

## 4.2 Experiment Matrix

Each cathode was tested with three different working gases; helium, helium plus 1% hydrogen and helium plus 1% oxygen. Film deposition was initially measured using a stylus profilometer. Measuring a thickness of less than 100 Angstroms requires calibrating an alternate technique, discussed later. We tested molybdenum, tungsten and two different types of carbon, pyrolytic and vitreous, both of which were recommended for vacuum application.

Table 3 shows the results of the matrix of experiments. Molybdenum with pure helium established our benchmark; 1917Å for the vertical position and 1624Å for the horizontal position. When we enriched the plasma with 1% hydrogen or oxygen the film thickness increased. With tungsten and pure helium the film thickness decreased almost a factor of two; 1097Å vertical, 1272Å horizontal. Although significant, this benefit would only slow down the accumulation of sputtered material and not resolve the performance or damage issues. Pyrolytic and vitreous carbons in an oxygen enriched gas gave us the expected results. When we attempted to measure the sputtered step after four hours of an oxygen enriched plasma, we were at the limit of resolution for the stylus profilometer with a float glass substrate. We repeated these experiments doubling the sputtered time, and again we were unable to measure a recognizable step: (<100Å).

| Cathode Material | Helium Gas Substrate Position | | Helium + 1% $H_2$ gas Substrate Position | | Helium + 1% $O_2$ Gas Substrate Position | | Sputter Time |
|---|---|---|---|---|---|---|---|
| | Vertical | Horizontal | Vertical | Horizontal | Vertical | Horizontal | |
| Moly | 1917 Å | 1624 Å | 2317 Å | 1718 Å | 3685 Å | 2761 Å | 240 min |
| Tungsten | 1865 Å | 1322 Å | | | | | 268 min |
| Pyrolytic Carbon | 1097 Å | 1272 Å | 2422 Å | 1343 Å | <235 Å | <100 Å | 240 min |
| Pyrolytic Carbon | | | | | <100 Å | <100 Å | 480 min |
| Vitreous Carbon | 2677 Å | 908 Å | 2160 Å | 818 Å | *<100 Å | *<100 Å | 260 min<br>*480 min |

• Minimum step resolution of stylus profilometer was 100 Å

**Table 3.** Measured film thickness on the witness substrate with different cathode materials and different working gases.

## 4.3 Calibration of Deposited Film

We were confident that this reactive gas process was limiting the deposition of carbon and it was essential that we quantify any deposit and effluent gasses. To measure film thickness of less than 100Å we used a non-contact laser interference microscope and re-measured the horizontal float glass substrate used when evaluating molybdenum cathode material and the oxygen enriched plasma. Table 4, row 1, compares the stylus measurement, 2761Å, with the Zygo phase measuring laser interferometric microscope, 2110Å on float glass. The Zygo 3-dimension surface map evaluation of

the float glass indicated that we could not expect a more precise comparison without flatter substrate material. We then used a silicon wafer with 20Å RMS surface roughness and compared the measured sputtered step height using the stylus profilometer, 1238Å and the Zygo interferometer, 1500Å, with calibrated Argon ion erosion rates for Auger electron spectroscopy (AES) 1563Å. After measuring several locations we were confident that we could measure thin films using the published erosion rates for carbon with the AES. We repeated the sputtering test again using vitreous carbon and an oxygen enriched plasma with a silicon wafer substrate. In Table 4, row 3, we compare the resolution limits of the Zygo interferometer with this substrate, 20Å, with calibrated argon ion erosion for the masked and unmasked surface, both 25Å.

| Cathode Material | Gas | Substrate Material | Measuring technique Stylus | Zygo | Auger | Time |
|---|---|---|---|---|---|---|
| Moly | Helium + 1% $O_2$ | Float glass | 2761 Å | 2110 Å | | 240 min |
| Vitreous Carbon | Helium | Silicon wafer* | 1238 Å | 1500 Å± 20 | 1563Å±10 | 250 min |
| Vitreous Carbon | Helium + 1% $O_2$ | Silicon wafer* | | <20Å | Front 25Å | 240 min |
| Vitreous Carbon | Helium + 1% $O_2$ | $SiO_2$ Laser Polished window | | no damage @1.06μm, 10ns | | 240 min |

*Surface limits 20Å

**Table 4.** Comparing film deposit measurements using auger ion erosion rates, Zygo laser interference microscope and a stylus profilometer. Fused silica laser window was damage tested after exposure to an oxygen enriched plasma using a carbon cathode.

## 4.4 Laser Damage Evaluation

We were fairly confident that the carbon measured was background contamination and not sputtered from the cathode. To prove this we replaced the substrate material with a 2 inch diameter laser-polished fused silica ($SiO_2$) window and repeated the sputtering test. After 4 hours of sputtering the $SiO_2$ window was removed and damage tested.[5] Laser-polished fused silica damages in excess of 60 J/cm$^2$ at 1064 nm with a 10 ns pulse width. We exposed several sites; all damaged at fluences in excess of the nominal threshold.

## 4.5 Confirmation of Reactive Gas Process

The remaining issue necessary to confirm the reactive gas process was to characterize the effluent gasses. Figure 5 is a schematic of the Materials Evaluation Experiment. This system was designed to characterize volatiles evolving from materials exposed to the pulsed plasma used in switching the Pockels cell. The system needed to accommodate a broad range of operating conditions and techniques necessary to identify decomposition of cell materials. The primary diagnostic used to document the reactive gas process was a quadrupole mass spectrometer residual gas analyzer (RGA). To achieve parts-per-million (ppm) sensitivity, it was essential for the RGA to operate at $< 1 \times 10^{-6}$ torr. The magnetically enhanced carbon cathode switched the Pockels cell most efficiently at about $5.0 \times 10^{-2}$ torr. By isolating the cell from the RGA and independently pumping both systems, we maintained optimum pressure while sampling the plasma effluence through the bypass metering valve.

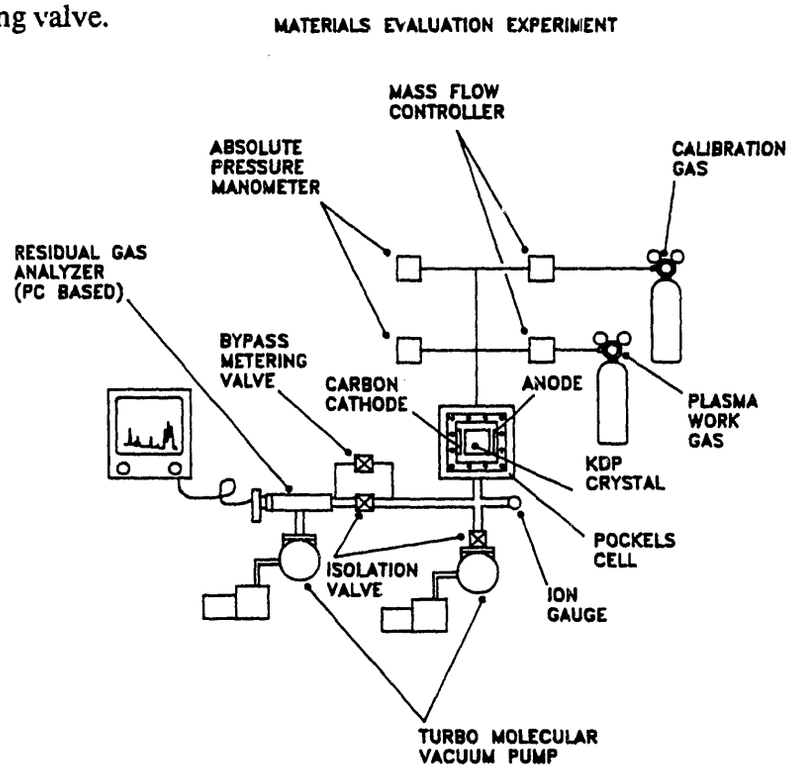


**Figure 5.** Schematic of the Materials Evaluation Experiment showing the Pockels cell, gas flow controls and the differentially pumped quadrupole mass spectrometer.

To optimize the resolution of the RGA with this differentially pumped technique, we monitored 10 ppm calibrated samples of oxygen ($O_2$) carbon monoxide (CO) and carbon dioxide ($CO_2$) in helium at switching pressures and adjusted the bypass metering valve for peak values. We easily resolved the 10 ppm levels of calibration gas and prepared the materials experiment apparatus to evaluate a carbon cathode with an oxygen-enriched plasma. Flowing 200 sccm of oxygen enriched

helium we maintained the cell pressure at $5.0 \times 10^{-2}$ torr. The pre-pulse DC glow discharge of 380 volts at 23 ma was followed by a 750 volt, plasma pulse running at 1 Hz. Sampling of the plasma effluence was continuous as we monitored the production of CO and $CO_2$, and varied the partial pressure of oxygen from 100 ppm to 10,000 ppm. We made several attempts to quantitatively balance the reaction; however, the differentially pumped geometry discriminates for mass species. Within this limitation, we were able to establish a mass balance within a factor of 2. We estimate that the carbon sputter rate under these conditions was about $1.1 \times 10^{16}$ atoms per second. This assumes singly ionized Helium bombarding the carbon surface with a sputter yield of 0.1. For a gas flow rate of 100 sccm to each half of the Pockels cell, we are delivering $8 \times 10^{15}$, $8 \times 10^{16}$, and $8 \times 10^{17}$ $O_2$ molecules per second for input concentrations of 100 ppm, 1,000 ppm, and 10,000 ppm, respectively (see Table 5).

| Initial $O_2$ Concentration (ppm) | $O_2$ input (Molecules/sec) | $CO + CO_2$ generation (Molecules/sec) |
|---|---|---|
| 100 | $8 \times 10^{15}$ | $1.4 \times 10^{16}$ |
| 1,000 | $8 \times 10^{16}$ | $4 \times 10^{16}$ |
| 10,000 | $8 \times 10^{17}$ | $7 \times 10^{16}$ |

**Table 5.** Generation rates of CO and $CO_2$ as a function of $O_2$ input to the Pockels cell. Carbon sputter rate due to the bombardment is established to be $1.1 \times 10^{16}$ atoms/sec.

Table 5 demonstrates that at this flow rate, oxygen concentrations above 100 ppm produce substantial chemical sputtering (direct reaction with the carbon cathode surface). Only at 100 ppm $O_2$ was the $CO/CO_2$ generation rate comparable to our estimate of He sputter rate due to helium bombardment. For this flow rate, 1,000 ppm $O_2$ would probably be sufficient to completely react with He-sputtered carbon.

Recent tests of the full aperture prototype Pockels cell,[6] with the carbon cathode and 1% oxygen enriched plasma, have shown that the cathode material has not deposited on the surface of the cell; and a $SiO_2$ substrate exposed during theses tests showed no change in the bulk damage threshold. Figure 6 records the deposition of cathode material for this test using a resonant frequency quartz crystal deposition monitor.

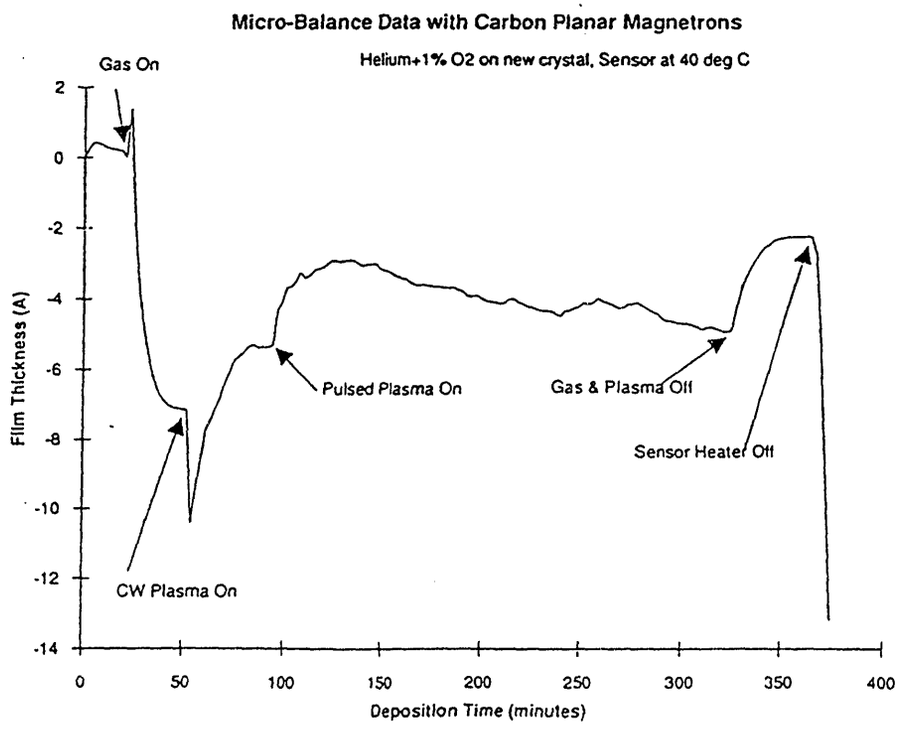


**Figure 6.** Plot of the deposited carbon film on a resonate frequency deposition monitor. 200 minutes of .25 Hz plasma pulse shows no measurable deposit.

## 4.6 Introduction to Carbon Graphite Cathode Materials

As we have mentioned, the use of a carbon cathode with a reactive gas has successfully resolved the damage and performance issues associated with the deposit of cathode material on the exposed cell surfaces. Apart from the electrical properties, Poco, and pyrolytic graphite and vitreous carbon were selected because of their high purity and associated physical properties.

Poco[7] graphite is electron beam evaporated; sized and processed to produce an ultrafine grain, high density, isotropic polycrystalline material with low inter-connecting porosity and can be purified to <5 ppm. Pyrolytic[8] graphite is manufactured by decomposition of a hydrocarbon gas at very high temperatures in a vacuum furnace. The product is ultra-pure, near theoretical density and extremely anisotropic. This anisotropy results from the layered hexagonal crystalline deposit characteristic of this process. Vitreous carbon[9] is obtained by carbonization and thermal treatment of organic material having strong transverse molecular bonds. The product has the characteristics of glass; it has a very high crystalline disorder with closed sub-microscopic spaces, impervious to gas, which gives it low density (1.5 $gcm^3$). All three of these carbon graphites were selected because their structures produce low vacuum outgassing characteristics.

Although each of these cathode materials performed well in the reactive gas process the final material selected will depend largely on the cathode geometry. Both Poco and pyrolitic graphite can be easily machined, however, pyrolitic material is not available in billet form. Vitreous carbon

resists oxidation and is commercially used as electrodes but has properties of glass and must be molded to the desired shape. We are currently developing a hollow cathode design for the prototype switch; the appropriate material and detailed design will be determined in the course of this effort.

## 5.0 Materials Evaluation Experiment Apparatus

As previously discussed, the Materials Experiment Apparatus was designed to evaluate cell materials exposed to the pulsed plasma and their affect on the optical performance of the Pockels cell. Plasma contamination, lifetime degradation, deposited volatiles, change in material properties are all issues we addressed in engineering the Plasma Electrode Pockels Cell (PEPC).

The Material Experiment Apparatus has 5 axes of movement for optical evaluation. (Figure 7 experiment photograph.) We have full control of flow and pressure, of both the plasma work gas and calibration gases. The plasma chambers are fabricated from ultra high vacuum machinable ceramic. Material samples to be tested are fabricated as part of the mid-plane exposed to the two low pressure plasma chambers. Access to plasma chambers for sampling deposited volatiles is through the optical windows. The system is portable and can be transported to the laser damage lab to damage test the crystal samples. Plasma gases are monitored using the differentially pumped RGA, discussed previously. Typical plasma lifetime exposures were performed using 380 v @ 23 ma pre-pulse glow discharge with 750 v, 1 Hz plasma pulse for $2.5 \times 10^5$ pulses. All samples were tested at $5.0 \times 10^{-2}$ torr flowing 1% oxygen enriched helium, at 200 sccm.

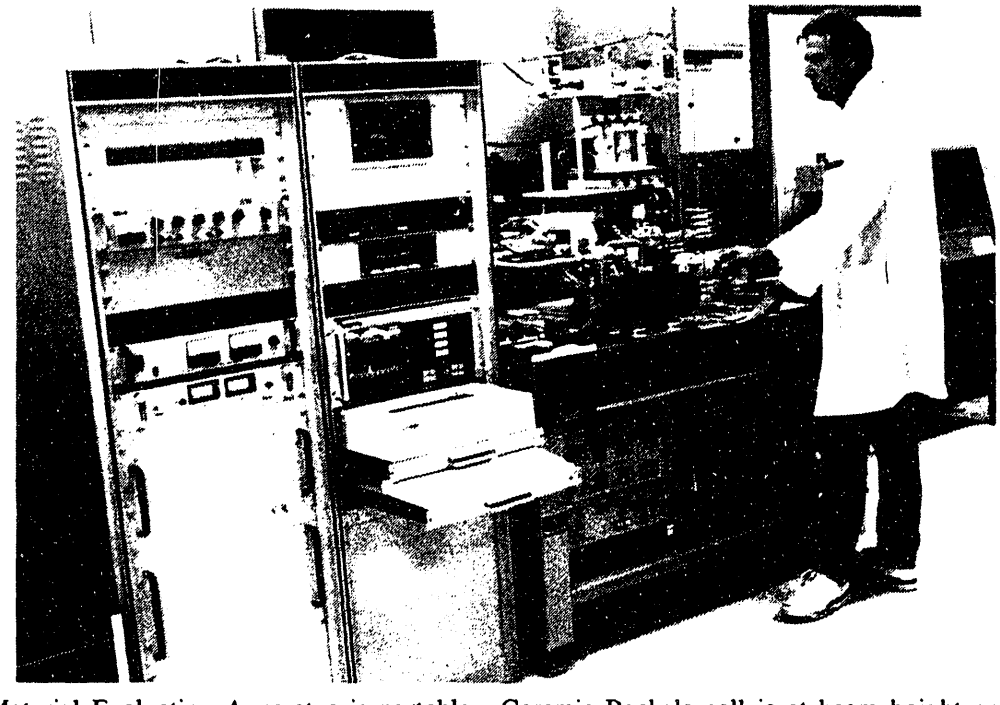

**Figure 7.** Material Evaluation Apparatus is portable. Ceramic Pockels cell is at beam height and the system can be transported into the laser damage facility or the optical polarimeter for performance evaluation.

## 5.1 Evaluation of the Silicone Encapsulant

Because of the physical size of the PEPC optical switch we concentrated our analysis on the available materials suitable for the construction of the prototype. The first material sample tested was the silicone encapsulant; Dow Corning 93-500 Space-Grade Encapsulant. A 7.0 cm X 7.0 cm sample was encapsulated in the center of the mid plane. (See Figure 8.) A silicon wafer witness substrate was positioned below the encapsulant where pumped volatiles or sputtered material would deposit. We continuously recorded RGA spectra of the plasma effluence and saw no change in the typical values for this discharge during the 2.5 X $10^5$ pulses.

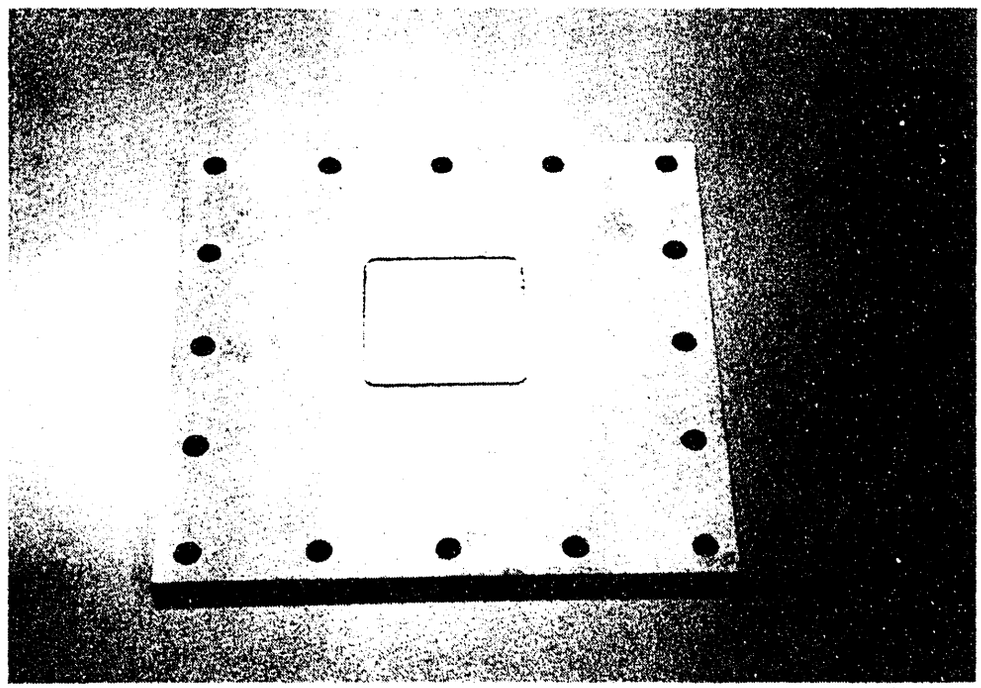

**Figure 8.** Photograph of the Pockels cell mid plane with a 7.0 cm X 7.0 cm patch of Dow Corning 93-500 Silicone prepared for testing.

### 5.1.1 Analysis

Analysis of the silicon witness substrate was done on a Perkin-Elmer 5400 ESCA System using x-ray photoelectric spectroscopy (XPS). Broad scan analysis of both the front and back surfaces were done for comparison, followed by higher-resolution scans of the elements to determine concentrations. The sample was alternately sputtered and analyzed to estimate the thickness of the surface. Sputtering was done using 4 kV $Ar^+$ ions. The sputtering rate had been previously calibrated to be 43 Å/min. Table 6 compares the atomic percent concentration of the exposed front

surface with the unexposed back surface. The plot graphically displays the depth profile of the atomic percent concentration as a function of ion sputtering time.

The unexposed back surface is the benchmark from which we compared all the materials tested. The oxide layer (O), absorbed hydrocarbons (C) and the silicon (Si) concentrations were typical for this substrate and type of surface-sensitive analysis. The minor trace deposit of chlorine (Cl) is a normal residue from the chlorofluorocarbon cleaning solvents, however, the trace gold (Au) is not typical and its source remains unresolved.

The exposed front surface has a nominal 20% increase in the oxide layer that was expected with the addition of oxygen to the discharge plasma. The increased carbon signal could be a component of the encapsulant, but is more likely surface contamination (when compared with the sputtering time of the other trace elements). Both the minor and major trace elements are not products of the silicone encapsulant, but are actually elements found in the analysis of the Mykrov and Macor cell materials, discussed below.

Perkin-Elmer 5400 ESCA
concentrations on 2nd witness plate for 93-500,
atomic percent

| | Fe | F | O | V | Ti | Ca | C | Cl | S | Si | Au |
|---|---|---|---|---|---|---|---|---|---|---|---|
| back | | | | | | | | | | | |
| as received | -- | -- | 41.0 | -- | -- | -- | 19.5 | 0.2 | -- | 39.1 | 0.2 |
| front | | | | | | | | | | | |
| as recieved | 4.5 | 1.0 | 52.2 | 2.4 | 0.4 | 5.7 | 24.3 | -- | 1.6 | 7.5 | 0.4 |
| after 20 seconds | 8.7 | 2.6 | 63.9 | 3.2 | 0.7 | 8.9 | -- | -- | 0.8 | 11.2 | 0.1 |
| after 40 seconds | 6.5 | 1.6 | 63.4 | 3.3 | 0.8 | 8.7 | -- | -- | -- | 15.5 | 0.1 |
| after 60 seconds | 4.8 | -- | 60.6 | 1.4 | 0.4 | 6.3 | -- | -- | -- | 26.4 | 0.1 |
| after 2 minutes | 1.6 | -- | 51.9 | -- | -- | 5.6 | -- | -- | -- | 41.0 | -- |
| after 3 minutes | 3.0 | -- | 21.9 | -- | -- | 1.9 | -- | -- | -- | 73.1 | -- |
| after 5 minutes | 1.2 | -- | 0.7 | -- | -- | -- | -- | -- | -- | 98.1 | -- |

Depth profile of major components on silicon witness

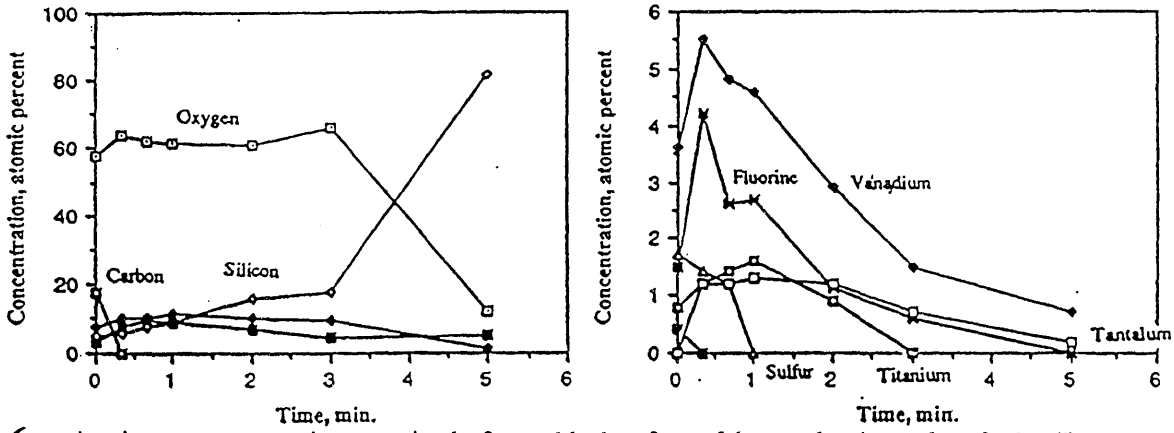


**Table 6.** Atomic percent concentration comparing the front and back surfaces of the sample witness plate, for the silicone encapsulant exposed to the plasma discharge. The plots graphically display the percent concentration as a function of ion sputtering time.

### 5.1.2. Effects of Ultra Violet Radiation

From both the RGA spectra and surface analysis there was no indication that the silicone encapsulant was decomposing. However, when we examined the exposed sample surface there was clear evidence of minor crazing and discoloration (Figure 9). This was not unexpected since published literature[10,11] for silicone rubber (polydimethylsiloxane) suggested that long exposure to vacuum ultra violet radiation (<290 nm) cleaves the methyl radicals to product $CH_4$, CO and $CO_2$,[12] and also fractures the C-H bond to produce atomic carbon. In the presence of an oxygen-enriched plasma we could expect the process to be limited because the exposed silicone atom would bond with free oxygen to produce $SiO_2$, thereby passivating the surface with minor shrinkage and a slight change in the physical properties. The structural formula of polydimethylsiloxane:

PDMS

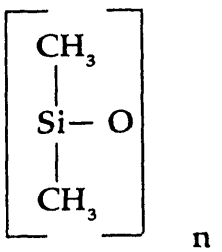

**Figure 9.** Dow Corning 93-500 silicone exposed to UV radiation of the pulsed plasma slightly crazes the surface. Cracks are superficial and nominally 3-4 μ wide.

### 5.1.3. Change in Physical Properties

Since we were aware there could be a change in material properties, we surveyed the durometer of the encapsulant sample before and after the exposure test. Using a Zwick Duro Test Stand we checked seven locations crossing both axes. Before exposure all points sampled were between 45-1/2 and 46 Shore-A hardness and agreed with the manufacturer's specification for properly cured material. After exposure for 2.5 X $10^5$ shots all points were nominally 15 percent higher in hardness. To see if this effect was superficial or a change in the bulk properties, the encapsulated silicone was removed from the mid-plane to survey the back surface. All points sampled were again 15 percent higher in hardness than before the exposure.

### 5.1.4 Effects of Ozone and Arcing

Although this bulk change is minor and should not affect the performance of the optical switch, we nonetheless decided to characterize the radiation from the plasma discharge. This material was specially formulated to resist the affects of UV radiation and ozone. Fracturing the strong C-H bonds was caused by heating rather than UV radiation.

### Analysis

We positioned a Jerrall-Ash scanning monochromator in front of the plasma discharge. With a wide range photo multiplier tube attached at the outlet split, we calibrated the experiment by identifying the intense 253.6 mm, 312.1 mm and 365.0 mm lines of a mercury vapor lamp. Using a 1% oxygen enriched pulsed discharge, we scanned the plasma spectra from 240 nm to 400 nm and recorded the results on a strip chart. Based on published line spectra for helium and oxygen we expected to see several strong lines in the near UV. However, our signals were weak and diffuse. Only the lines above 388.8 nm of helium appeared sharp and characteristic. We rechecked our calibration and repeated the experiment with pure helium only. The line spectra was sharp and typical for helium in the near UV. We repeated both discharge experiments several times; Figure 10 shows the addition of oxygen leads to a reduction in the emitted UV intensity.

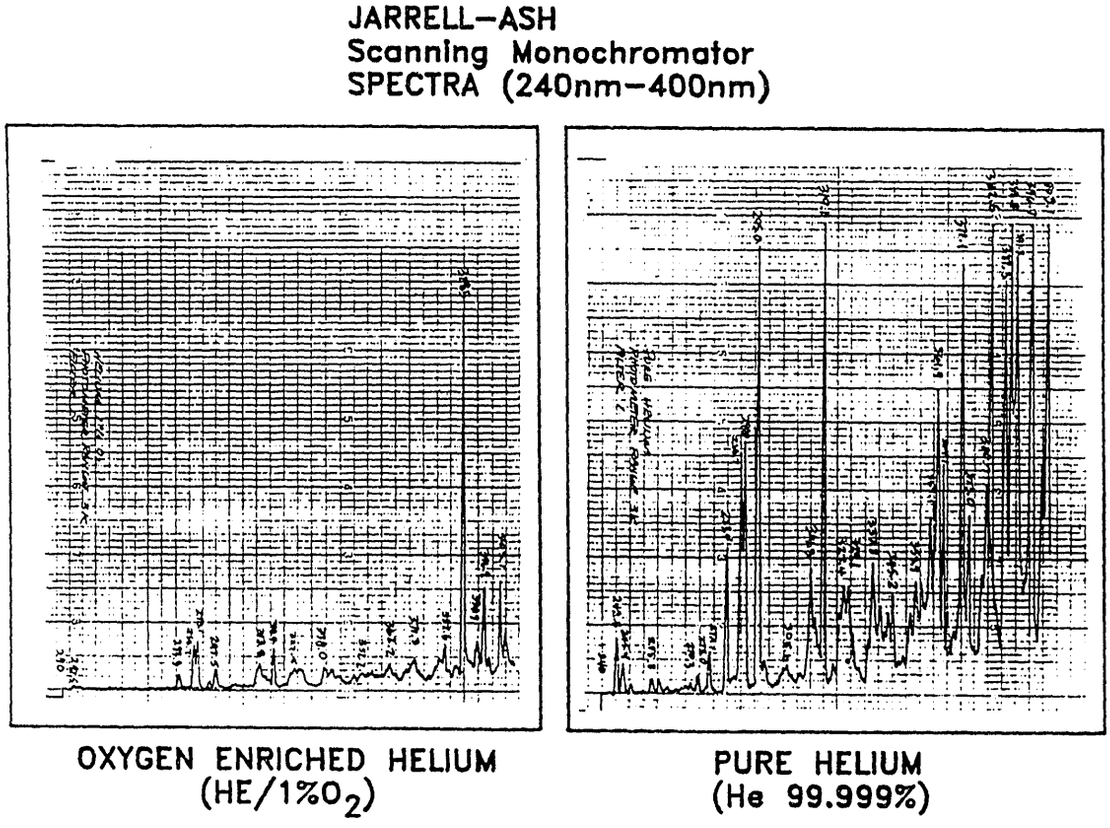


**Figure 10.** Strip chart of the line spectra shows the addition of oxygen to the plasma produces ozone and absorbs the ultra violet (UV) radiation. When oxygen is removed the characteristic UV spectra of helium appears.

In the vacuum ultra violet (VUV), the absorption of ozone ($O_3$) is almost entirely continuous.[13] Apparently the addition of oxygen to the plasma not only completes the reaction for the hydrocarbon volatiles but produces ozone that absorbs in the VUV and limits the VUV emission from the cell. The resistance of polydemethlsiloxane (PDMS) to oxygen and ozone attack is primarily chemical. Residual carbon to carbon double bonds (C=C) in polymers are the major locus of attack.[14] The absence of such bonds in PDMS is the primary reason of resistance to these gases.

Silicone is almost completely resistant to the action of oxygen and ozone on natural aging and even very high concentrations have no serious affect.[15] The strongest indication of discoloration was closest to the discharge cathode; a closer examination of the mid-plane and the sample indicated the evidence of arcing. Although we made no attempt to measure the plasma temperature, it was clear

the electrode geometry was primarily the reason for discoloration. Alternate cathode designs have already been considered and can easily eliminate this problem. The issue of UV decay is also well understood and is generally addressed by pigmenting the silicone, although for our application it does not appear necessary. The addition of an absorber like 2-hydroxybenzophenone and others are extensively used to protect surfaces from UV degradation.

## 5.3 Evaluation of Macor and Mykroy Switch Materials

The next material investigated was the Mykroy.[16] Mykroy is one of the primary structural materials considered for the optical switch. We currently have fabricated the material evaluation apparatus cell from Macor,[17] a material similar to Mykroy, because of the low permeation and outgassing properties (see Table 1) required for these tests. Both materials are composed of two-phase randomly oriented fluorophlogopite micro crystals in a glass matrix. Fluorophlogopite ($K_2Mg_6(Al_2Sl_6O_2)F_4$) is a synthetic mica and for the purpose of this evaluation both these materials are chemically the same, although, there is a significant difference in the mechanical and electrical properties. To test the Mykroy it was only necessary to install a mid-plane fabricated from the material. The experimental parameters have been previously discussed and both the RGA and silicon witness substrate were used in the analysis of the material.

### Analysis

The RGA spectra did not reveal any evidence that the Mykroy changed the effluent gasses which are characteristic of this plasma discharge. The synthetic fluorophlogopite (Mykroy) structure and composition is well documented; potassium (K), magnesium (Mg), aluminum (Al), silicon (Si), oxygen (O) and fluorine (F) are the basic elements. Table 7 tabulates the XPS analysis of the witness substrate. The table compares the percent composition of the unexposed back surface, with the deposited volatiles on the exposed front surface, and records the atomic percent concentration as a function of the time the deposited film is sputtered. The deposition of iron (Fe), vanadium (V), titanium (Ti) and calcium (Ca) is not typical of fluorophlogopite and was detected throughout most of the deposited film.

Perkin-Elmer 5400 ESCA

Compositions on mykroy witness plate,

atomic percent

| | Fe | F | O | V | Ti | Ca | C | P | Sr | Al | Si | S |
|---|---|---|---|---|---|---|---|---|---|---|---|---|
| mykroy -back | | | | | | | | | | | | |
| as received | -- | -- | 46.4 | -- | -- | 0.3 | 14.4 | -- | -- | -- | 39.0 | -- |
| mykroy -front | | | | | | | | | | | | |
| as recieved | 1.4 | 1.2 | 41.4 | 6.3 | 0.7 | 10.6 | 27.1 | 0.6 | -- | 2.3 | 7.3 | 1.1 |
| after 0.5 minutes | 3.5 | 2.0 | 60.7 | 5.9 | 1.3 | 13.0 | 0.9 | -- | -- | 2.8 | 10.0 | -- |
| after 1.0 minutes | 3.6 | 1.9 | 61.0 | 5.9 | 1.4 | 13.5 | -- | -- | -- | 2.1 | 10.6 | -- |
| after 2.0 minutes | 3.8 | 1.8 | 61.3 | 5.1 | 1.7 | 13.0 | -- | -- | -- | 2.2 | 11.1 | -- |
| after 3.0 minutes | 4.1 | -- | 61.0 | 4.6 | 1.6 | 13.5 | -- | -- | -- | 2.2 | 13.1 | -- |
| after 5.0 minutes | 5.2 | -- | 56.9 | -- | 0.4 | 11.5 | -- | -- | -- | -- | 25.9 | -- |

**Table 7.** Atomic percent concentration of material evolving from the Mykroy mid plane. Table compares the front exposed surface with the unexposed back surface of the sample witness plate.

To establish the origin of these elements, we analyzed virgin samples of both Mykroy and Macor using a spectral emission technique. Table 8 is a spectrochemcial analysis, comparing the concentration by weight in ppm for Macor and Mykroy. The analysis is semiquantitative; the numbers cited are the concentration required to confirm the elements presence. The reported values are typically within +/-50% of the actual value.

The major components of the mica, borasilicate glass and all of the trace elements on the witness substrate were detected.

SPECTROCHEMICAL ANALYSIS REPORT

Analytical Chemistry Section

| "MACOR" Mica Crystal & Glass | | | Mykroy plate | | |
|---|---|---|---|---|---|
| Element | Not Detected | Found (ppm) by weight | Element | Not Detected | Found (ppm) by weight |
| Si | | =>5000 | Si | | =>5000 |
| K | | =>5000 | K | | =>5000 |
| Mg | | =>5000 | Ca | | =>5000 |
| B | | =>5000 | Ba | | =>5000 |
| Al | | =>5000 | Na | | =>5000 |
| Ca | | 3000 | Mg | | =>5000 |
| Na | | 3000 | B | | =>5000 |
| Sn | | 300 | Al | | =>5000 |
| Ba | | 100 | Pb | | 2000 |
| Fe | | 100 | Sr | | 1000 |
| P | | 100 | Fe | | 1000 |
| Ti | | 100 | Li | | 300 |
| Li | | 30 | P | | 300 |
| Rb | | 30 | Rb | | 300 |
| Zr | | 30 | Ti | | 100 |
| Ga | | 30 | Zr | | 100 |
| Pb | | 20 | Mn | | 30 |
| Sr | | 10 | Cr | | 30 |
| Mn | | 10 | Ga | | 20 |
| V | | 10 | V | | 20 |
| Cu | | 8 | Cu | | 8 |
| | | | Be | | 1 |

**Table 8.** Spectrochemical analysis of Mykroy and Macor cell materials. Both materials contain the trace elements found on all the sample witness plates.

Subsequent conversation with the manufacturer of Mykroy indicated they typically use 99.9% pure chemicals to produce their synthetic mica and vary the concentration and composition of the glass matrix to obtain the correct physical properties. The two-phase glass and micro crystal structure is produced by ball milling the mica and hot pressing to the finished product. Both the processing and the purity of starting chemicals can easily account for the addition of these impurities.

## 5.4 Evaluation of Polyethylene Switch Cell Material

The next material investigated was ultra high molecular weight (UHMW) polyethylene. Although polyethylene only has fair mechanical properties it was available in the dimensions necessary to fabricate the prototype switch. The experimental parameters have been previously discussed. The entire mid-plane was again fabricated from UHMW polyethylene. The silicone witness substrate and the RGA were again used to monitor decomposition and volatiles. The likely evolution of water ($H_2O$) and hydrocarbons from polyethylene were difficult to detect with the oxygen enriched plasma and there was no change in the characteristic RGA spectra of the discharge during the life-time exposure of $2.5 \times 10^5$ pulses.

### 5.4.1 Analysis

Surface analysis of the silicon witness substrate was again performed using XPS. Figure 11 is the characteristic plot of atomic percent concentration verses ion sputtering time of the deposited material. Again we see the strong oxide layer typical of the oxygen enriched plasma and the trace elements characteristic of cell materials.

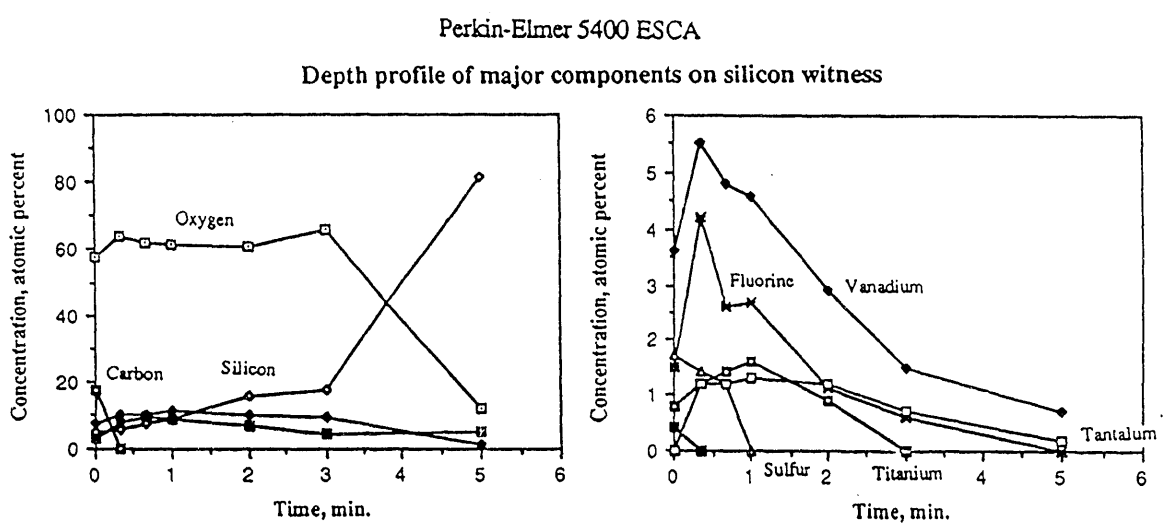


**Figure 11.** Graphic display of the atomic percent concentration of deposited cell materials when evaluation the polyethylene. Trace elements are deposited through the entire oxide layer.

### 5.4.2 Effect of Discharge Arcing

Figure 12 (photo of polyethylene mid-plane) reveals the effect of arcing when polyethylene is exposed to the discharged plasma. The discoloration in the surface follows the outline of the plasma chamber but is most evident on the cathode side. The analysis of the silicon witness substrate showed no evidence of a hydrocarbon deposit. This was expected because the oxygen enriched plasma reacts with the volatiles and the product is pumped away. Experiments conducted with the prototype polyethylene cell[18] and a hydrogen discharge measured decomposed cell material on a silicon witness substrate using XPS analysis. There is no reason to assume we could not detect the decomposed hydrocarbon if the oxygen were not present during these tests.

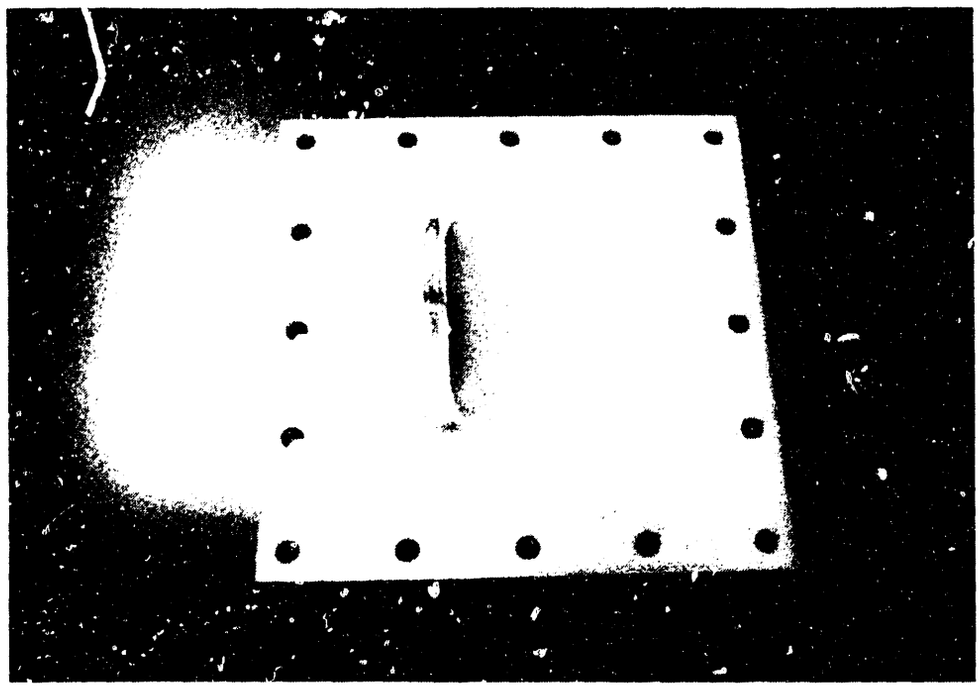

**Figure 12.** Photograph of the polyethylene mid-plane reveals the affect of arcing when exposed to the discharged plasma.

## 6.0 Conclusion

This evaluation was not intended to be an exhaustive survey of the best possible materials for the construction of the optical switch. Rather, it was a prudent effort to ensure that the materials selected would not affect the fair evaluation and performance of the switch, or develop into a major maintenance issue affecting the experimental schedule of the Beamlet project.

The initial materials surveyed and the approach we used to evaluate them were based on the recommendation of the inventors, scientists and engineers involved in the project. It is fair to say that many of our concerns associated with the reactive properties of the plasma and switch material were legitimate. The evolution of volatiles, the affect of UV radiation, erosion and decomposition of materials were all issues we had anticipated. The actual construction and testing of the prototype switch help to define the operating parameters and narrow the scope of our evaluation. Once the working gas, pressure and switch voltage were defined many of the materials issues were addressed by manipulating them rather than eliminating them.

The structural integrity of the switch will be largely dependent on the final geometry. Materials like polyethylene, with a low creep modulus, must be engineered carefully. For an arrayed architecture, where the electrode location would result in minimizing material cross-section, casting the electrodes and high voltage leads in a mica glass composite should be investigated.

In the final analysis all the materials surveyed have limitations and carefully monitoring the Beamlet prototype will ensure that we maintain a conservative approach in developing a switch for the NOVA upgrade.

## 6.1 Acknowledgments

Much of the work reported was in reaction to unanticipated problems. Our success was in large part due to the expertise of those who supported us. Special thanks to P. Biltoft and M. Benapfl for their analysis and support in resolving the cathode sputtering issues; B. Woods for his support in mapping and characterizing the strain induced birefringence of the encapsulated KD*P crystals; F. DeMarco for optical damage measurements. T. Demiris, M. Schildbach, A. Connor, C. Evans and E. Lindsey for their support in quantifying surface deposits of the materials investigated. M. Rhodes, J. Taylor and D. Burns for the many hours of electronic design and support of the Materials Evaluation Test Facility.

## References


1) J. Goldhar, M. Henesian, Large Aperture Electro-Optical Switch and Plasma Electrodes, IEEE J. Quantum Electronics QE-11, 1137 (1986)
2) AVS Standard, Jour. of Vac. and Tech. Vol 2, no. 6 Dec. (1965) AVS 9.1-1964
3) H. Hayakawa, M. Umino, H. More and Y. Tujii, Observations of Striations in Nd:YAG with Circular Polarized Light, Jap. J. Appl. Phys. Vol 24 pp. L614-L616, (1979)
4) Beamlet Optical Switch Development Group Memo: To Atherton, May 1992, "Documentation of procedure for encapsulating the 32 cm KDP Crystal".
5) A.J. Morgan, F. Rainer, F.P. DeMarco, R.P. Gonzales, M.R. Kozlowski, M.C. Staggs. NISP, Spec. Pub. 801 p.47-57 (1989) Expanded Test Facilities at LLNL
6) M.A. Rhodes, B.W. Woods, J.J. DeYoreo, L.J. Atherton, Very Large Aperture Optical Switch for Advanced NOVA Lasers, UCRL-MI-108694
7) Poco Graphite Inc. Unocal Company, 1601 South State Street, Decatur, TX 76234
8) Union Carbide Advanced Ceramics, Pure Tech Inc., P.O. Bos 1319, Caramel, New York, 10512
9) Carbone of American, Ultra Carbon Division, 900 Harrison St., Bay City, MI 48708
10) Space Mater. Handbook, 3rd edition, 11.4.5, Affect of Solar Radiation
11) Plym. Mater. Sci. Eng. 56, 469 (1987)
12) C.W. Lentz Ind. Res. and Dev., April, 139 (1980)
13) W.C. Price, D.M. Simpson, Trans. Far. Soc. 37, 106 (1941)
14) M.D. Beers, Handbook of Adhesives, 2nd edit., Reinhold Co., New York, 1977, p.631
15) W. Noll, Chem. and Tech. of Silicones (501) 9.6.3, Resistance to Ozone and Weather
16) THERMICA-MYKROY's trade name for Fluorophlogopite Synthetic mica
17) G.H. Beale, Advances in Nucleation and Crystallization of Glasses, Amer. Cer. Soc. Spec. Publ. No. 5 (Freiman, Columbus, 1971) p.251. MACOR trademark of Corning Glass Works
18) M. Rhodes, B. Woods, Beamlet Rev., April (1992) PEPC Sputtering Update

DATE
FILMED
9/10/93

END